

● *Original Contribution*

HYPERTHERMIA BY MAGNETIC INDUCTION: I. PHYSICAL CHARACTERISTICS OF THE TECHNIQUE

JAMES R. OLESON, M.D., PH.D.

Division of Radiation Oncology, Arizona Health Sciences Center, Tucson, AZ 85724

Several electromagnetic techniques are currently used in hyperthermia therapy for cancer. This report discusses the magnetic induction technique, in which application of an alternating magnetic field to a conductor results in induction of eddy current flow and power deposition via ohmic losses. The power density in tissues depends upon the heterogeneous tissue conductivities and dielectric constants, magnetic field intensity and distribution, and eddy current radius. Using a newly developed magnetic field probe, the magnetic fields produced at 13.56 MHz by electrodes of a commercial magnetic induction device have been accurately mapped and used to calculate power densities in static phantoms. Calculated and observed temperature elevations in a cylindrically symmetric phantom agree well, confirming the simple formula in this case relating power density to magnetic field strength. The efficiencies of three commercially available electrodes have been accurately measured using calorimetric techniques and phantom loads modeling human anatomy and electrical conductivity. The effect of eccentric positioning of the load has been studied using magnetic field mapping techniques. Power densities in a very simplified model of human anatomy that retains cylindrical symmetry were calculated. Effects of inhomogeneities in conductivity have been investigated qualitatively using composite static phantoms modeling human cross-sectional anatomy and thermographic camera recordings of surface temperature distributions. The advantages and disadvantages of this heating technique are discussed from the point of view of the power density distributions in heterogeneous materials. Evaluation of power density distributions is essential for optimizing this heating technique using various electrode arrangements and/or load modifications, for providing part of the information needed for solution of the bioheat transfer equation in living subjects, and for predicting the ability of the technique to heat specific tumors.

Hyperthermia, Magnetic induction, Radiofrequency diathermy, High frequency diathermy.

INTRODUCTION

Many different techniques are being investigated for producing hyperthermia in biological tissues as an anti-cancer agent.¹⁶ For local or regional heating, these include microwave applicators and interstitial antennae, ultrasound, and high frequency (HF), either capacitively or inductively coupled. Both high frequency magnetic induction and microwaves were applied as diathermy techniques in physical medicine in the 1930's. Mortimer and Osborne¹⁴ emphasized then the difficulty in physically characterizing "deep heating" in living subjects using HF diathermy; techniques for measuring temperatures in deep body sites and for accurately measuring and mapping strong HF magnetic fields are only now being developed. Attempts to characterize the power density in tissues have in the past been based upon rather crude calorimetric techniques. Pätzold and Wenk,¹⁷ in an effort to study the biophysics of this technique, attempted to measure relative power deposited by magnetic induction

in concentric layers of materials having varying electrical conductivities. Modern use of HF magnetic induction for "deep" heating in cancer therapy is exemplified in the work of Storm et al.,^{19,20,21} who report significant temperature elevations in tumors at unspecified depths heated with a 13.56 MHz coil concentric with the longitudinal body axis. The physical characteristics of this heating technique, including power density measurements, are extremely important in defining its advantages and disadvantages, and form the subject of this investigation. We describe results of accurate and precise mapping of the magnetic field produced by electrodes associated with a 13.56 MHz generator; calculation of power density and temperature in homogeneous non-perfused phantoms; comparison of calculated and measured temperatures in these homogeneous phantoms; measurement of electrode efficiencies by calorimetric means; properties of eddy current distributions in loads eccentrically placed within the body electrode; power density calculations for repre-

Supported in part by National Cancer Institute Grant CA17343 and in part by an Arizona Health Sciences Center Biomedical Research Support Grant.

Presented in part at the Bioelectromagnetics Society Meeting, Washington, D.C., August 10, 1981.

Acknowledgements—The author thanks Anne Fletcher and

Winifred Vincent for assistance in conducting several experiments, Kathy Grochowski for preparation of illustrations, and Sue McFarland for typing this manuscript. T. C. Cetas has contributed greatly through frequent discussions.

Accepted for publication 7 June 1982.

sentative volumes of human subjects; and thermometric representations of power densities in heterogeneous static, i.e., unperfused, phantoms modeling human cross-sectional anatomy.

METHODS AND MATERIALS

High frequency generator and electrodes

A 13.56 MHz generator* was used for all magnetic induction experiments reported here. Three electrodes were supplied with the generator, all having a cylindrical shape. The body electrode had a radius of 24.75 cm and a length of 28.6 cm. The thigh electrode radius was 11 cm and its length was 7.9 cm. The neck electrode radius was 11 cm and its length was 1.9 cm. All applied power measurements were done with a dual HF power sensor† incorporated into the generator, and were done under conditions of zero reflected power.

Magnetic field probe

A newly developed vector HF magnetic field (H) probe based upon photoammeter principles was used for all magnetic field measurements.¹⁵ The probe is minimally field perturbing and measures field intensity over a 2 cm² area. The H² versus power relationship for the probe is linear with a correlation coefficient of 0.9998. The precision in field intensity is ± 1% of full-scale value, which is 300 A/m. A calibration scheme has been developed that yields an accuracy within 5%, consistent with values deduced from calorimetry experiments and measurements with an isotropic field probe.‡

Conductivity measurements

Conductivities and dielectric constants of phantom materials were measured with a probe of the design described by Hahn *et al.*,¹¹ together with a RF Vector impedance bridge.* Calibration of the probe using published data²² for saline solutions of known molarity resulted in conductivity values accurate to ± 5%. Probe polarization effects may result in much larger errors in measurement of dielectric constants.²²

Phantom materials

The phantom modeling materials developed by Guy¹⁰ have been adjusted for appropriate conductivity and approximate dielectric constants at 13.56 MHz. Specific mixtures and electrical values are given in Table 1. The electrical conductivities and dielectric constants reported by Hahn *et al.*¹¹ for pig tissue have been used as representative of human tissue. For the magnetic field mapping measurements and electrode efficiency measurements, cylindrically symmetric containers of saline were used. This allowed for measurement of magnetic fields *within*

the load, and for stirring to achieve temperature uniformity in the calorimetric efficiency studies. The conductivity in each of these saline loads at 23°C was 0.69/Ω · m, modeling human muscle at 13.56 MHz. In the case of the thigh and neck electrodes, a load of radius 7.75 cm and length 14 cm was used, and in the case of the body electrode, the load radius was 14.25 cm and the length was 31.1 cm. Thus these loads approximately modeled the physical dimensions of the body regions that normally would be heated with the respective electrodes.

Temperature measurements

Temperatures within phantom materials were measured during periods of interruption of HF power with polytetrafluoroethylene sheathed copper-constantan thermocouples† and a clinical thermometer.‡ Junction temperatures were read to ± 0.1°C, but measurement in a region of thermal gradient of order 1°/cm may have led to additional uncertainty of ± 0.1°C because of inaccurate placement of the thermocouple junction in the material. Surface temperatures were recorded with a thermographic camera.§ This technique together with an error analysis has been described in detail by Cetas.³

Power density formulae

A formula can be derived analytically for power deposition in a cylindrically symmetric load aligned coaxially with a cylindrical sheet conductor (electrode). A coordinate system ($\hat{r}, \hat{\theta}, \hat{z}$) is defined such that the cylindrical electrode has its axis along (0, 0, \hat{z}), and the electrode ends are at $z = \pm L/2$. Current at angular frequency ω passing through the electrode creates a magnetic field (units of A · m⁻¹) within the electrode

$$\vec{H} = \vec{H}_0(r, \theta, z)e^{i\omega t}.$$

Faraday's law in integral form is

$$\oint \vec{E} \cdot d\vec{l} = \frac{-\partial}{\partial t} \int \mu_0 \vec{H} \cdot \vec{n} dS,$$

where \vec{E} is the induced electromotive force, $d\vec{l}$ is a line element along a closed contour, and \vec{n} is a unit vector normal to the surface element dS .¹² Because of the assumed cylindrical symmetry $\vec{E} = E\hat{\theta}$ and

$$\oint \vec{E} \cdot d\vec{l} = 2\pi r E = -i\omega\mu_0 \int_0^r H_z(r') 2\pi r' dr',$$

so

$$\vec{E}(r) = -\frac{i\omega\mu_0}{r} \hat{\theta} \int_0^r H_z(r') r' dr'.$$

*Henry Medical Electronics, Los Angeles, CA.

†Bird Electronic Corp., Cleveland, Ohio.

‡Model HI 3002, Holaday Industries, Inc., Eden Prairie, MN.

*Model 4815A, Hewlett Packard, Palo Alto, CA.

†IT-18 thermocouples and TM-10 thermometer, Bailey Instr. Inc., Saddle Brook, NJ.

‡UTI Spectrotherm Corp., Sunnyvale, CA.

Table 1. Recipes for phantom materials at 13.56 MHz

| Tissue | Composition, % by weight | Dielectric constant ϵ | Conductivity σ (ohm \cdot m) ⁻¹ | Specific heat | Density |
|----------------------------------|--|-----------------------------------|--|---------------|---------|
| Muscle (skeletal and cardiac) | 0.5% NaCl 90% H ₂ O 9.5% TX-150 jelling agent† | 80 | 0.69 | 0.91 | 1.0 |
| Viscera (liver and bowel) | 0.26% NaCl 90% H ₂ O 9.7% TX-150 jelling agent | 80 | 0.43 | 0.91 | 1.0 |
| Lung | 82.15% polyester resin* 16.65% aluminum powder 1.19% acetylene black MEK catalyst | 38 | 0.12 | .35 | 1.30 |
| Fat and bone | 83.71% polyester resin* 14.9% aluminum powder 1.37% acetylene black MEK catalyst | 28 | 0.23 | .35 | 1.30 |

*"A-1" clear casting resin, A-1 Paint and Varnish Co., Torrance, CA 90509. Available at all "Standard Brands" Stores.

†Available from Oil Center Research, P.O. Box 51871, Lafayette, LA 70505.

Note: ϵ and σ are measured values at 23°C designed to model those determined by Hahn *et al.*¹¹ ϵ values used here may be lower than actual tissue values by a factor of about two: See discussion in Ref. 22 regarding the probe polarization effects.

We have assumed above that the permeability of biological loads is that of free space, $\mu_0 = 4\pi \times 10^{-7}$ Volt \cdot sec/A \cdot m.

The power density (W/m³) is

$$P_v(r) = \frac{1}{2} \sigma E E^* = \frac{\sigma \omega^2 \mu_0^2}{2r^2} \left[\int_0^r H_{\theta\theta}(r') r' dr' \right]^2 \quad (1)$$

E^* is the complex conjugate of E and σ is the electrical conductivity of the load in 1/ $\Omega \cdot$ m. In the case of a magnetic field uniform across a plane perpendicular to the z axis,

$$P_v(r) = \sigma \omega^2 \mu_0^2 H_{\theta\theta}^2 r^2 / 8. \quad (2)$$

The effect of the linear dependence of conductivity σ upon temperature can be included explicitly in formulae (1) and (2) with appropriate modifications (P.F. Turner, written communication, April, 1980).

The radial dependence of the magnetic field of a homogeneous, cylindrically symmetric load inside a cylindrical electrode has been recently solved analytically by Young *et al.*,²³ and is shown to depend upon both conductivity and dielectric constants of the material. The effect of a finite dielectric constant upon power deposition is small for body tissues at 13.56 MHz, as assumed in using a constant value for $H_{\theta\theta}$ in Eq. 2.

Temperature calculations

Conversion of power density into temperature rise, in the case of pulsed heating of a static phantom in which thermal conduction may be ignored, is accomplished using the formula

$$\Delta T = P_v \Delta t k / \rho C \quad (3)$$

where ΔT is the temperature rise in °C, P_v is the power density in W/m³, Δt is the time in seconds during which power is applied, k is a units conversion factor, C is specific heat, and ρ is the density of the load.

Human subjects

Magnetic fields were measured during treatment of several human subjects using the body electrode. All human subjects had biopsy-proven malignancies and had signed informed consent forms for treatment approved by the Arizona Health Sciences Center Human Subjects Committee.

RESULTS

Magnetic field maps

Maps of the amplitude of the z -component of the magnetic field of the neck, thigh, and body electrodes are shown in Fig. 1-3 respectively. The neck and thigh electrode maps were obtained with 600 watts applied to loads described above, and the body electrode map was obtained with 900 watts applied. No significant compo-

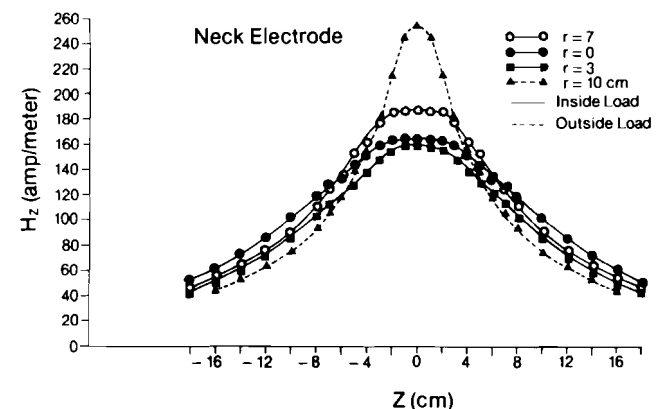


Fig. 1. Magnetic field map of the neck electrode.

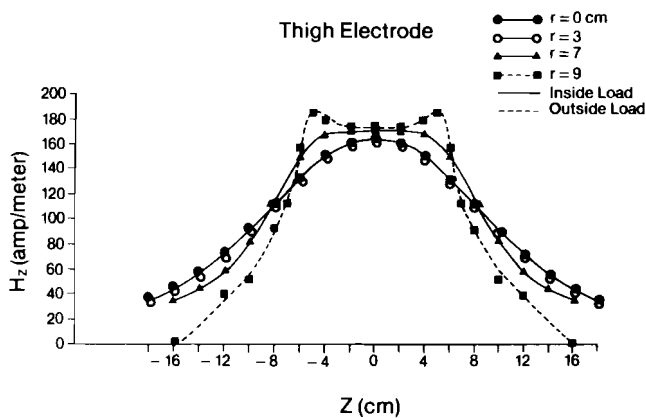


Fig. 2. Magnetic field map of the thigh electrode.

ment of the magnetic field in directions orthogonal to the z direction was observed with the magnetic field probe within the body electrode. The magnetic field within the load varies radially by only 5% in the case of the body electrode.

Power density measurements

A cylindrical phantom of radius 22.75 cm and length 8.1 cm was placed coaxially within the body electrode. The phantom composition was 90% distilled H₂O, 0.6% NaCl, and 9.4% jelling agent.* This gave a measured conductivity of 0.82/Ω · m at 23°C. The specific heat of the material was determined by the method of mixtures to be 0.91. Power at 800 watts was applied for four minutes. The magnetic field measured across the surface of the phantom, the measured temperatures along a radius in the midplane of the phantom, and the temperatures calculated from the measured conductivity and magnetic field using Eq. 1 are shown in Fig. 4. Included in the calculation was the effect of a 2% per °C increase in conductivity as the phantom heated, as verified by direct measurements in separate experiments. All error bars shown represent ± 2 standard deviations (S.D.) for all random error sources. The anomalously low temperature

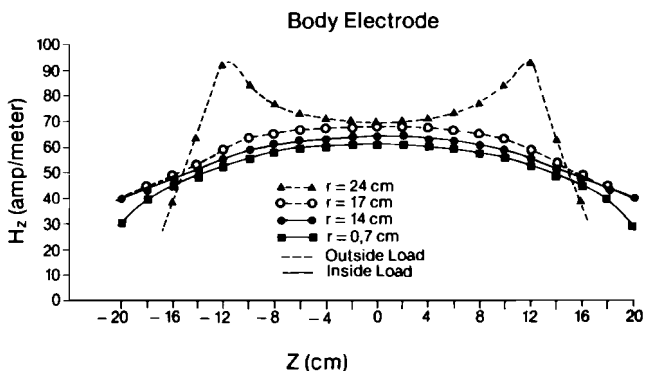


Fig. 3. Magnetic field map of the body electrode.

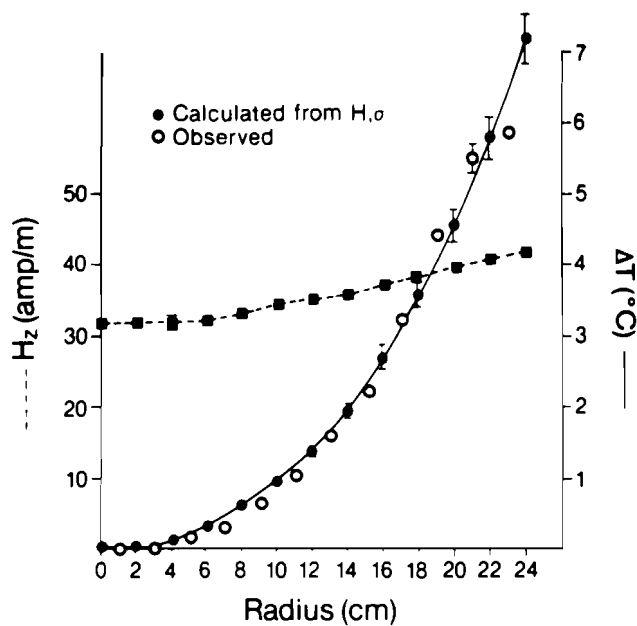


Fig. 4. Observed and calculated temperatures resulting from heating in the measured magnetic field shown.

measured near the outer edge of the phantom was because of heat loss to the surrounding air as well as to thermal conduction within the phantom. The measured and calculated temperatures (and therefore power densities) agreed within stated errors.

Electrode efficiencies

Calorimetrically determined efficiencies (100% × power dissipated in the load ÷ power applied to the electrode) were 76% ± 2% for the thigh, 55% ± 2% for the neck, and 83% ± 2% for the body electrode, respectively.

Power density variation with eccentric load positioning

The saline load appropriate for the body electrode as described above was used to study the effect of eccentric load placement. The magnetic field was measured along the diameter common to both the body electrode and the load as shown as the line "d" in Fig. 5, for both a centered and an eccentric load position. The applied power was 900 watts. As a measure of the change in superficial power deposition relative to deep power deposition, the ratio of magnetic field at the center of the load (points A and C, resp., in Fig. 5) to the field at the periphery of the load (points B and D, resp.) was calculated: H(A)/H(B) = .94 (centered load) and H(C)/H(D) = .82 (eccentric load). Because of the increasing field strength near the electrode, eccentric placement of the load exposed the superficial portion of the load nearest the electrode to a more intense field, relative to the load centered situation; this resulted in greater superficial power deposition. We note that a load simulating the body must be used to study this

*TX-150, available from Oil Center Research, Lafayette, LA.

effect. gradie oppos magn ing, t posit

Calcu

Me applic about posit proba at a g patie body surfa 55 A heati

Us vice 13.5 result and base the tom The A/m the n 6.

In ann surf show affec tion Blo

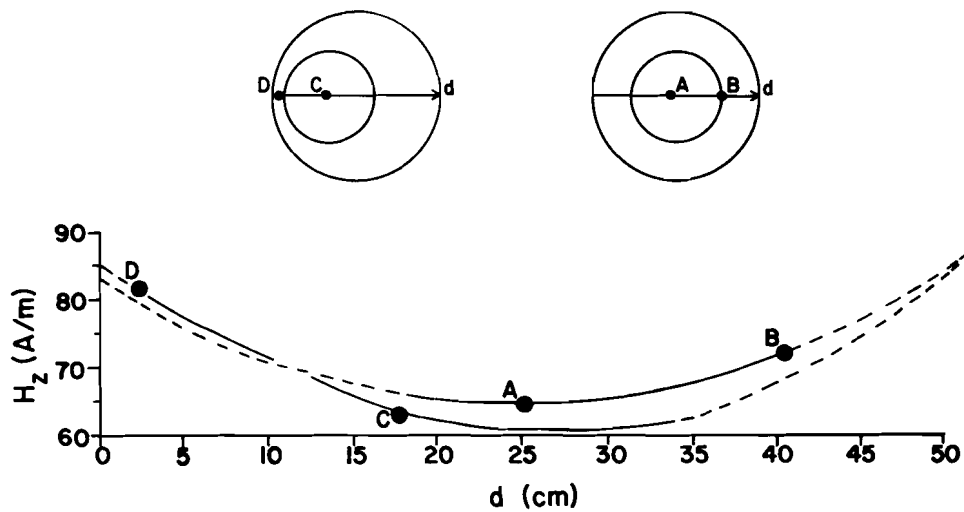


Fig. 5. Magnetic fields along diameters of a load eccentrically positioned as well as centered in the body electrode.

effect. When physically smaller loads were used, the gradients in the magnetic field varied and a conclusion opposite to that above resulted in some cases. Were the magnetic field uniform and unchanged with load positioning, there would be no change in power deposition with position.

Calculated power density in human subject

Measured magnetic fields at the body surface at given applied power were reproducible in a given patient within about $\pm 7\%$ from treatment to treatment. Variation in positioning the electrode along the longitudinal body axis probably accounted for this variation. The magnetic field at a given applied power varied somewhat from patient to patient depending upon body shape, muscle mass, and body region. With 600 watts applied power, typical surface magnetic fields were 72 A/m for pelvic heating, 55 A/m for abdominal heating, and 65 A/m for thoracic heating.

Using values of tissue conductivity of $0.45/\Omega \cdot m$ for viscera, $0.2/\Omega \cdot m$ for fat, and $0.69/\Omega \cdot m$ for muscle at 13.56 MHz, we calculated the power density that would result in a load having concentric annuli of fat, muscle, and viscera, respectively. The radii of the annuli were based upon those giving cross-sections of the same area as the elliptical cross-sections measured with computed tomography for the pelvic region of a particular patient. The magnetic field observed in this same patient (80 A/m) with an applied power of 600 W was also used, and the resulting power density distribution is shown in Figure 6.

In this case the power density peaks in the muscle annulus at typical depths of 2 to 5 cm below the skin surface, and the central power density is zero. This model shows generally how the varying tissue conductivity affects power density, giving relatively less power deposition in the subcutaneous fat than in the muscle annulus. Blood perfusion would be expected to produce tempera-

ture gradients much smaller than the power density gradients. An advantage of this model over more complicated ones is that the power density can be calculated *analytically* and used together with the bioheat transfer equation to model the effects of perfusion. On the other hand, this model does not account for the heterogeneities within each annulus, such as bone masses that would divert the eddy current flow and create local volumes of power density (and temperature) increased or decreased from that shown. In the next section we describe results of studying these heterogeneities with a more realistic model.

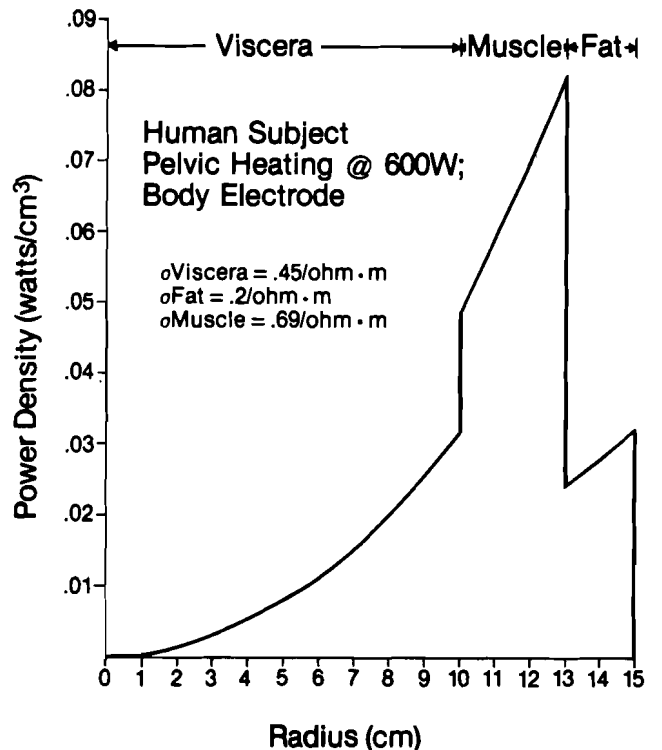


Fig. 6. Power density distribution calculated for concentric annuli as a simplified model of human anatomy.

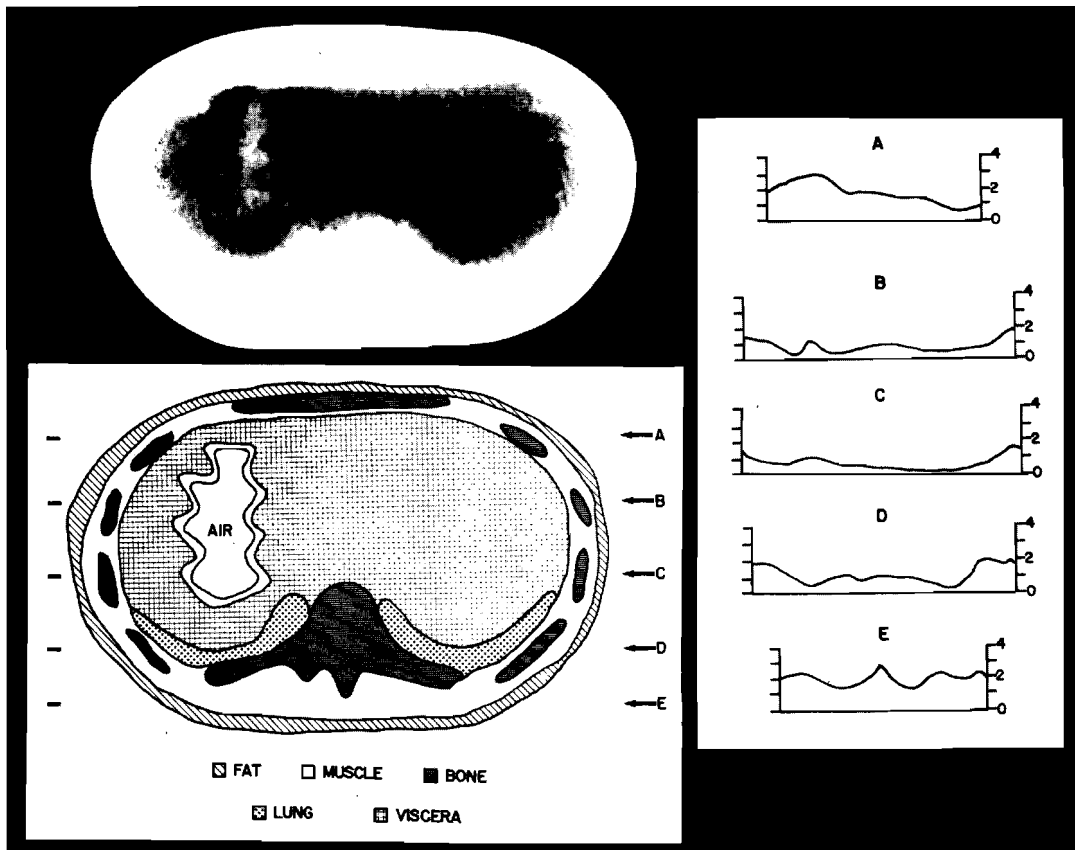
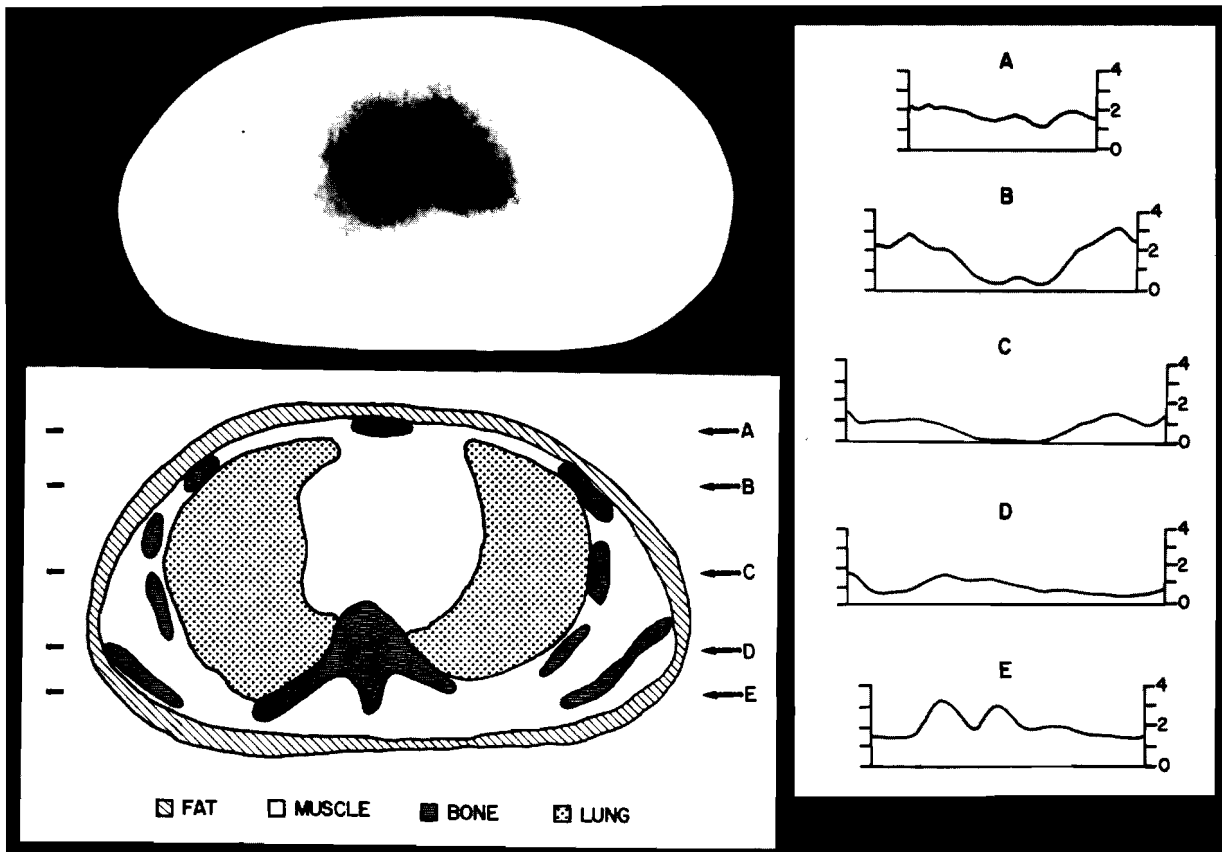


Fig. 7. From top to bottom: line drawings and a surface thermogram for phantoms of cross-sectional human anatomy at the levels of the mid-thorax (A), upper abdomen (B), high pelvis (C), and low pelvis (D), respectively. The temperature distribution along each of the horizontal levels indicated by lettered fiducial marks is shown to the right of each thermogram. The scale of temperature elevation above baseline temperatures is shown for each temperature distribution. The horizontal scale of distance on each temperature distribution is one-half the distance scale of the line drawings and thermograms.

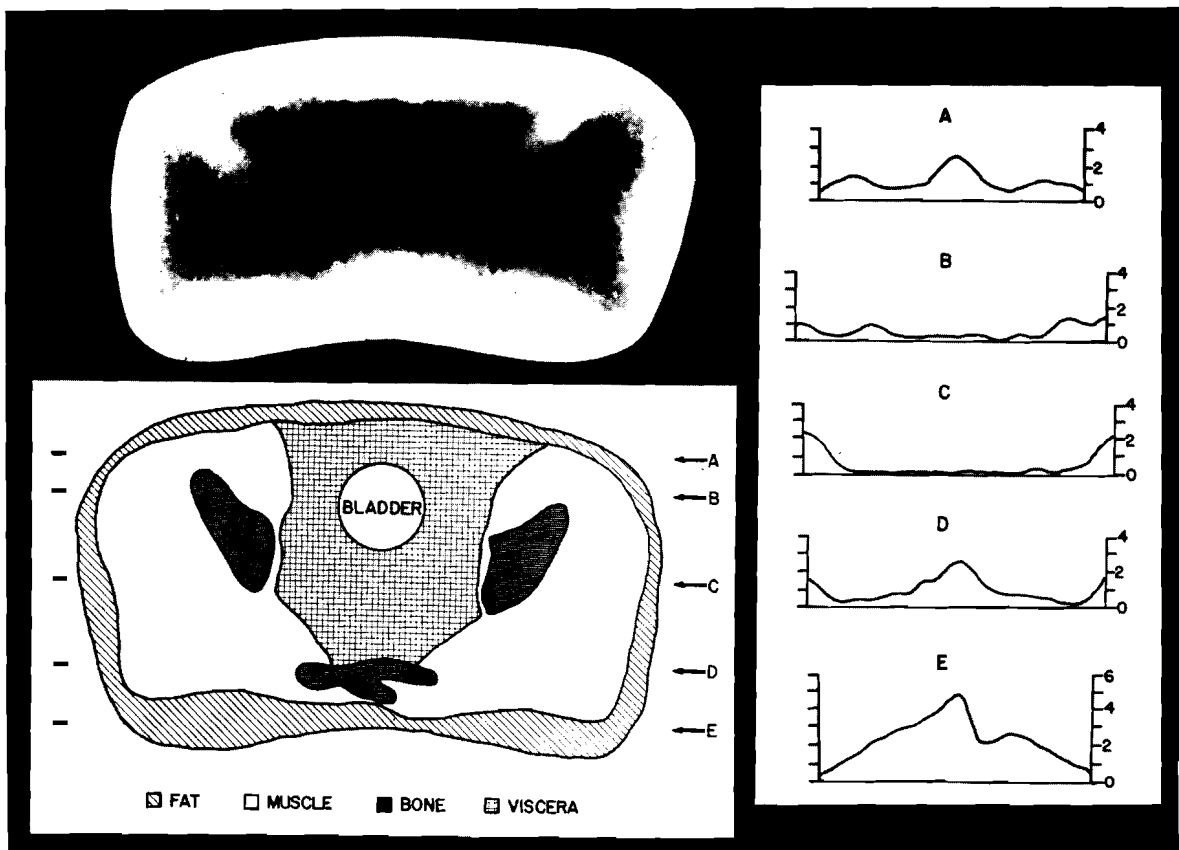
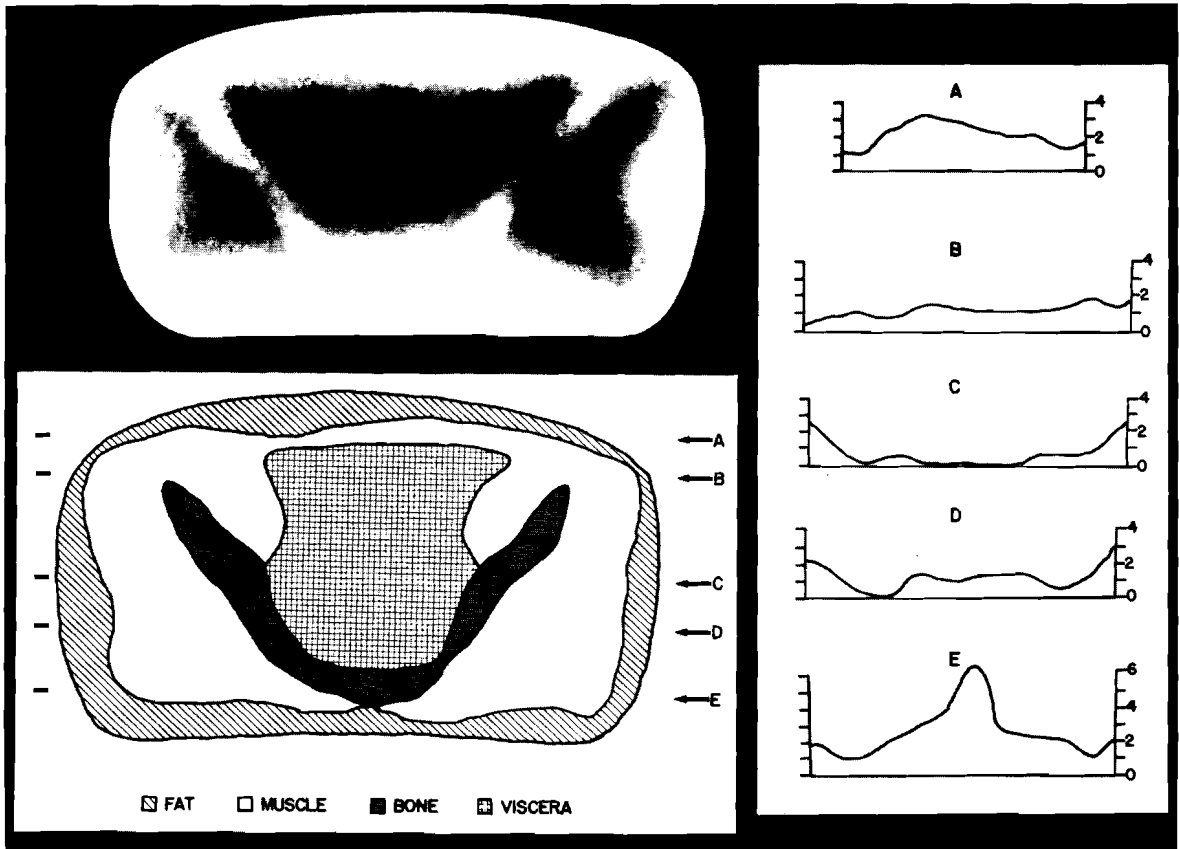


Fig 7. Continued.

Power densities in phantoms of human cross-sectional anatomy

Four static phantoms, each 3 cm thick, accurately modeling the electrical conductivity of tissue volumes in humans, were constructed according to cross-sectional anatomic geometry (Fig. 7A-D). These representations were taken from a standard atlas of cross-sectional anatomy at levels of mid-thorax, upper abdomen, high pelvis, and low pelvis. Each of these phantoms was heated using the body electrode together with a saline load that provided proper electrical loading for the electrode. A power level of 1 kW was applied for three minutes in each case. The resulting thermograms are shown in Fig. 7A-D along with line drawings of the respective sections. The magnetic field gradient from the center to the periphery of these phantoms was slightly more than that shown in the magnetic field map in Fig. 3. In particular, the measured magnetic field amplitudes (A/m) at the center and greatest radius of the phantoms were 58.8; 65.7 for the thorax, 58.3; 66.8 for the abdomen, 58.3; 68.9 for the high pelvis, and 57.2; 63.6 for the low pelvis, respectively. Calculation using equations 2 and 3 with the mean radius of 13 cm gave a temperature rise of approximately 2.4°C for the outermost fat layer in the high pelvis phantom. A temperature of 2.5°C was observed thermographically, as seen on the center scan (C) for this phantom in Fig. 7C. The observed temperature was fortuitously in agreement with the calculation, but significant variations in temperature are noted in all phantoms at a given depth because of the heterogeneous electrical properties (e.g. scan E on Fig. 7A and scan E on Fig. 7C shows variation in temperature by a factor of two to three at similar depths). Transformation of the observed temperature elevations in Fig. 7 into power density may be done using Eq. 3. We show this in Fig. 8 only for the central scan (C) of the high pelvic section (Fig. 7C). The complex distribution of power density is easily appreciated, but it is important to note that the general features of zero to minimal power density at the center of the section ($r = 0$) and maximal power density in the outermost 5 cm of the phantom are

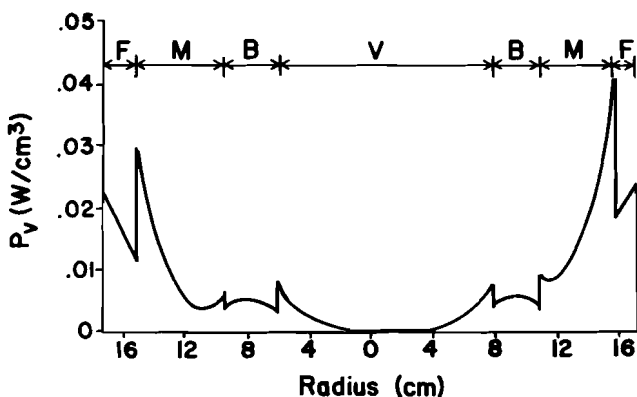


Fig. 8. Power density along the mid-level scan (C) on the high pelvis thermogram in Fig. 7C obtained by transformation of the corresponding temperature elevations using Eq. 3.

consistent with the calculated results for the simplified annular geometry (Fig. 6). Intense heating patterns occur at several noteworthy sites such as (i) at posterior superficial areas where eddy current flow around vertebral bodies causes high current densities in the subcutaneous fat layers; (ii) in the anterior portion of the lungs and chest wall; and (iii) in the anterior portion of the low pelvis.

DISCUSSION

Analysis of the bioheat transfer equation, as in the work of Bowman,² shows that elevation of tumor temperatures above that of surrounding normal tissues depends both upon the power density and blood perfusion rate in tumor relative to normal tissue. Perfusion rates in tumors, especially those with large areas of necrosis, tend to be lower than that of normal tissues and may be further lowered by hyperthermic effects.^{1,5,7,8,18} The perfusion rate of a specific tumor cannot be predicted *a priori*. With a given heating technique, however, the power density distribution in tissues may have predictable features that can serve as the basis for evaluating the advantages and disadvantages of a specific heating technique independently of tumor blood perfusion considerations. In the case of a heating technique that results in temperature elevations regionally as well as systemically, the existence of upper limits on temperatures tolerated by the organism implies the existence of upper limits on total applied power and power densities (for a given rate of heat loss from the organism). If it can be shown that a particular technique produces no direct power deposition in a volume, then the temperature increase of that volume will be the result only of perfusion by heated arterial blood and by thermal conduction from adjacent volumes, ignoring changes in metabolically produced heat. If this were the situation in a volume containing tumor, impaired perfusion of the tumor relative to normal tissue would be a disadvantage because of the longer time required for equilibration of tumor temperature with adjacent normal tissue temperatures. Alternatively, spatial variation of power density within a tumor having a given perfusion rate will lead to non-uniform heating of the tumor. In this case, practical difficulties in measuring temperatures at only a few points in humans may lead to erroneous conclusions regarding adequacy and uniformity of tumor heating. This issue is crucial, since Dewhirst, *et al.*,⁴ have shown recently that the probability of eradicating a tumor with heat and radiation depends upon the *minimum* time-temperature integral within the tumor. Using spontaneous tumors in pet dogs and cats, they showed that the proportion of complete responses was strongly temperature dependent between 42°C × 30 minutes and 45°C × 30 minutes. In addition, the cure rate was significantly higher in tumors heated at 44°C × 30 min. (75%) than in tumors heated at 43°C × 30 min. (37%).

The principal goal of this work is to study the power

density distribution obtained in tissue using high frequency magnetic induction with concentric electrodes. The power density with this technique depends upon tissue electrical conductivities and dielectric properties, upon the geometry of the load, and upon the amplitude and frequency of the applied magnetic field. In cases where the eddy current distribution is known analytically, accurate measurements of electrical conductivity and magnetic field strength lead to accurate determinations of power density. In the case of a cylindrically symmetric load, this power density is highly non-uniform even if the applied magnetic field is completely uniform, and is zero at the center of the load.

Evaluation of the power density distribution of phantoms designed to accurately model the electrical properties of a human cross-sectional anatomy shows that the power density in a heterogeneous load is very complicated. In such loads we cannot yet calculate the eddy current distribution analytically, so that measurement of tissue conductivities and magnetic field strengths is not sufficient for accurate description of the complex distributions. On the other hand, approximate values of power density based upon measured magnetic fields and a model using cylindrical symmetry and annular distributions of tissue types do fit the power density observed in the heterogeneous phantoms in an average sense: power density still peaks in the superficial muscle annulus (2–5 cm depth) and vanishes at the phantom center. A strong variation of tumor temperature elevations with depth of the tumors should be observed. In the only published work utilizing this heating technique,^{19,20,21} the temperature-depth correlations are not reported. The power density distribution obtained with this technique is disadvantageous for preferential heating of tumors or portions of tumors extending much more than 5 cm below the skin surface.

The suggestion is sometimes made that eccentric placement of the load within a concentric electrode will alter the eddy current distribution in such a way that the power density at depth can be increased relative to that at the body surface. Results reported here, using a body-equivalent phantom and magnetic field mapping, show that this is not the case. If the magnetic field were uniform, eccentric placement of the load would lead to no change in

eddy current distribution. Because the field strength increases near the inner surface of the electrode, only the eddy currents at large radii passing through the superficial tissues link this increased magnetic flux. The power density thus increases in superficial tissues near the electrode relative to deep tissues. In clinical practice, eccentric positioning of the subject is counter-productive since this results in hotter superficial spots and forces a reduction in total applied power. The density at depth ultimately is lower than with the subject centered in the electrode.

The study of power density patterns may help identify sites of possible excessive heating in normal tissues that should be monitored thermally. Furthermore, patterns of excessive heating could then be related to toxicity patterns observed with heat and radiation. Relatively high power densities near the spinal cord, for instance, may produce temperatures that significantly lower the radiation tolerance of the spinal cord.^{6,9,13} Monitoring adjacent paraspinal muscle temperatures during inductive heating could underestimate the actual cord temperatures.

Power density distributions, as observed here in phantoms that model human cross-sectional anatomy, will be useful in numerical studies of this heating method with the bioheat transfer equation. Such work is being done by Dr. R. Roemer at the University of Arizona, Department of Mechanical Engineering.

In summary, this work shows that the power density distribution obtained with magnetic induction using a concentric electrode peaks in the superficial portion of the load, even in the case of a heterogeneous load. Ability of the technique to heat tumors preferentially thus depends upon tumor depth, with greatest efficacy for tumors confined to a depth of 2–5 cm. Temperatures achieved deeper than this are determined principally by the temperature of the arterial perfusate, and these may have a predictable relationship to systemic temperatures. Investigation of this relationship is in progress.

The correlation between these studies of power density distributions and observed temperatures in normal tissues and tumors in the case of dogs and humans will be reported in a subsequent paper. Defining depths at which tumors are observed to be heated to $\geq 43^\circ\text{C}$. will be the principal goal of the second part of this work.

REFERENCES

1. Bicher, H.I., Hetzel, F.W., Sandhu, T.S., Frinak, B.S., Vaupel, P., O'Hara, M.D., O'Brien, T.: Effects of hyperthermia on normal and tumor microenvironment. *Radiology* **137**: 523–530, 1980.
2. Bowman, H.F.: Heat transfer mechanisms and thermal dosimetry. *J. Natl. Cancer Inst.* (In press).
3. Cetas, T.C.: Practical thermometry with a thermographic camera: Calibration, transmittance and emittance measurements. *Rev. Sci. Instrum.* **49**(2): 245–254, 1978.
4. Dewhirst, M.W., Moon, T., Carlin, D.: Analysis of tumor volume and thermal dosimetric effects on tumor response to heat, radiation, and heat plus radiation: Results of a phase III randomized clinical trial in pet animals. Presented at the AAPM Summer School, "Physical Aspects of Hyperthermia," Dartmouth College, Hanover, N.H., August 3–7, 1981.
5. Dewhirst, M.W., Ozimek, E.J., Gross, J., Cetas, T.C.: Will hyperthermia conquer the elusive hypoxic cell? *Radiology* **137**: 811–817, 1980.
6. Douglas, M.A., Parks, L.C., Bebin, J.: Sudden myelopathy secondary to therapeutic total-body hyperthermia after spinal-cord irradiation. *N. Engl. J. Med.* **304**: 583–585, 1981.
7. Eddy, H.A.: Alterations in tumor microvasculature during hyperthermia. *Radiology* **137**: 515–521, 1980.
8. Emami, B., Nussbaum, G.H., TenHaken, R.K., Hughes,

- W.L.: Physiological effects of hyperthermia: Response of capillary blood flow and structure to local tumor heating. *Radiology* **137**: 805-809, 1980.
9. Goffinet, D.R., Choi, K.Y., Brown, J.M.: The combined effects of hyperthermia and ionizing radiation on the adult mouse spinal cord. *Radiat. Res.* **72**: 238-245, 1977.
 10. Guy, A.W.: Analyses of electromagnetic fields induced in biological tissues by thermographic studies on equivalent phantom models. *IEEE Trans. on Microwave Theory and Techniques* **MTT-19**: 205-214, 1971.
 11. Hahn, G.M., Kernahram, P., Martinez, A., Pounds, D., Prionas, S., Anderson, T., and Justice, G.: Some heat transfer problems associated with heating by ultrasound, microwaves, or radiofrequency. *Ann. NY. Acad. Sci.* **335**: 327-345, 1980.
 12. Jackson, J.D.: *Classical Electrodynamics*. New York, John Wiley and Sons, Inc., 1962.
 13. Miller, R.C., Leith, J.T., Veomett, R.C., Gerner, E.W.: Potentiation of radiation myelitis in rats by hyperthermia. *Brit. J. Radiol.* **49**: 895-896, 1976.
 14. Mortimer, B., Osborne, S.L.: Tissue heating by short wave diathermy. *JAMA* **104**: 1413-1419, 1935.
 15. Oleson, J.R.: An accurate probe for mapping strong HF magnetic fields. *IEEE Trans. Biomed. Eng.* **8**: 581-583, 1982.
 16. Oleson, J.R., Gerner, E.W.: Hyperthermia in the treatment of malignancies. In *Therapeutic Heat and Cold*, 3rd edition, J.F. Lehmann (Ed.). Baltimore, Williams & Wilkins, 1982, pp. 603-635.
 17. Pätzold, J., Wenk, P.: Zur Wirkungsweise des Spulenfeldes in der Kurzwellentherapie: Wärmemessungen an geschichteten Elektrolyten im hochfrequenten Spulenfeld. *Strahlentherapie* **55**: 692-707, 1936.
 18. Song, C.W., Kang, M.S., Rhee, J.G., Levitt, S.H.: The effect of hyperthermia on vascular function, pH, and cell survival. *Radiology* **137**: 795-803, 1980.
 19. Storm, F.K., Harrison, W.H., Elliott, R.S., Hatzitheofilous, C., Morton, D.L.: Human hyperthermia therapy: Relationship between tumor type and capacity to induce hyperthermia by radiofrequency. *Amer. J. Surg.* **138**: 170-174, 1979.
 20. Storm, F.K., Harrison, W.H., Elliott, R.S., Morton, D.L.: Normal tissue and solid tumor effects of hyperthermia in animal models and clinical trials. *Cancer Res.* **39**: 2245-2251, 1979.
 21. Storm, F.K., Harrison, W.H., Elliott, R.S., Morton, D.L.: Hyperthermia therapy for human neoplasms: Thermal death time. *Cancer* **46**: 1849-1854, 1980.
 22. Toler, J., Seals, J.: RF dielectric properties measurement system, human and animal data. Cincinnati, US Department HEW (NIOSH) publication no. 77-176, 1977.
 23. Young, J.H., Wang, M.T., Brezovich, I.A.: Frequency/depth-penetration considerations in hyperthermia by magnetically induced currents. *Electron Letters* **16**: 358-359, 1980.